Title - Preclinical evaluation of artemether loaded polymeric nanorods for the treatment of malaria

Introduction

Malaria is one of the most menacing infectious diseases causing hugely contributing to the morbidity and mortality of human life around the globe. It was the third most contributor of the human life loss in the year 2019 accounting for a total of 4,10,762 human lives [1]. The disease is caused by the protozoa *Plasmodium*. *Plasmodium* life cycle consists of two phases namely the mosquito host and the human host. Mosquito being the primary transmitting host, the consequences of the disease are observed all over the globe and are so severe that in the year 2020, it was estimated that about half of the world's population was at the risk of malaria [2]. After the mosquito bite, the parasite enters the human body and proliferates at two major sites which happen to be the liver and the erythrocytes. The erythrocytic stage of the malaria is symptomatic [3] and most of the antimalarial drugs are intended to act on this erythrocytic stage of the parasite.

Currently WHO recommends artesunate in case of severe malaria. Intravenous artesunate is prescribed until the patient gains consciousness and is able to continue with the Coartem® (artemether and lumefantrine) therapy. Artesunate lacks a long half-life due to which the effective plasma drug concentration is achieved for a very short periods of time. This results in only partial inhibition of the parasites in the blood. The metabolism of artesunate varies in case of diseased individuals. Hence the prediction of the plasma concentration may be arbitrary amongst different patients. Currently there is no substitute to artesunate [4].

In order to ameliorate the drawbacks of artemisinin derivatives, various nanocarriers have been developed and utilized by the research groups. In order to enhance the solubility, PEGylated dendritic micelles have been used by Bhadra et. al. [5] while artemether-lumefantrine emulsion was developed by Yufan Ma and group, who also demonstrated the enhanced efficacy of the lipid emulsion [6]. Further, to improve the bioavailability and the plasma residence time, Isacchi et. al. formulated plain and PEGylated liposomes and demonstrated the long blood circulation time [7]. Similarly, nanosponges have also been observed as a suitable nanocarrier for improving the kinetics of artemether [8]. Apart from all of these, solid lipid nanoparticles and nanostructured lipid carriers have been widely utilized as a carrier for artemether. They have been employed for topical delivery [9], oral delivery [10], intranasal delivery [11], intraperitoneal delivery [12,13] and other parenteral deliveries [14,15]. Polymeric and related nanoparticles loaded with artemisinin and its derivatives have been formulated by various research groups and have been found to have improved kinetics as compared to free drug [16–20]. Apart from this, polymeric nanoparticles have advantages such as sustained and extended drug release profile, feasibility of various routes of administration, greater drug loading capacity etc.

All above researchers have tried to develop novel formulation with an aim for dose reduction, increased efficacy, reduction in parasitaemia, reduction in toxicity, specific organ targeting, formulate stable formulation, achieve controlled release of drug and achieve acceptable route of administration. However, to the best of our knowledge, no researcher has tried the approach of nonspherical particle delivery technique for achieving longer durations of plasma drug concentrations. Researchers have demonstrated the promising effects of nonspherical carriers in phagocytosis bypass [21], particle-cell interaction [22], cellular uptake mechanism and kinetics [23], tissue distribution of particles [24], margination of the particles in the blood vessels [23] and

intracellular distribution of the particles [25]. In this work we intend to formulate long-acting release rod shaped polymeric particles for the delivery of artemether. It is hypothesized that the drug loaded rod shaped particles once administered parenterally would maintain plasma drug concentrations for longer period of time which will release drug in a sustained manner.

Objectives

1) Fabrication, optimization and characterization of artemether loaded polymeric nanorods
2) Evaluation of cytotoxicity, haemolysis and drug release from artemether loaded polymeric nanorods
3) Preclinical evaluation of artemether loaded polymeric nanorods for antimalarial efficacy

Material and Methods

Material

Artemether (>98.0%) was purchased from Tokyo Chemical Industry Co. Ltd. (Tokyo, Japan). Poly(lactic-co-glycolic) acid (PLGA) (50:50, MW 30,000–60,000) and (75:25, MW 4000–15,000), polyvinyl alcohol (PVA, MW 9000–10,000) and coumarin-6 were purchased from Sigma-Aldrich Chemicals Company (Missouri, United States). Glycerol was purchased from S D Fine-Chem Ltd (Mumbai, India). Silicon oil was purchased from RankemTM (Bangalore, India). Trehalose was purchased from Spectrochem (Mumbai, India). Emplura® grade acetone was procured from Merck Life Science Pvt. Ltd. (Mumbai, India). Glutaraldehyde (25% w/w), EDTA and curcumin (internal standard) were purchased from HiMedia Laboratories Pvt. Ltd. (Mumbai, India). XenoLight 1,1′-dioctadecyl-3,3,3′,3′-tetramethylindotricarbocyanine iodide [DiR, (DilC18(7)] was procured from PerkinElmer (Waltham, United States). Water was obtained from Milli-Q system (Millipore GmbH, Germany). All other chemicals, solvents, and reagents utilized were either HPLC or analytical grade.

Method

Fabrication of artemether loaded polymeric nanospheres

Artemether (ART) loaded polymeric nanorods were prepared using nanoprecipitation technique. Various combinations of the polymer, surfactant and drug ratios were tried and optimized to yield desired particle size, %drug entrapment and %drug loading. Briefly, 10mg of ART and 75mg of PLGA were dissolved in 15ml acetone which comprised the organic phase while, 150mg of PVA was dissolved in warm Milli-Q water (65ºC) which comprised the aqueous phase. The organic phase was added to the aqueous phase under constant stirring (400rpm). The solution mixture was further subjected to reduced pressure using rotary vacuum evaporator (Buchi Rotavapor, Switzerland) until complete evaporation of acetone. The obtained nanosphere suspension was centrifuged at 20,000rpm for 40min to separate the nanospheres from the aqueous phase. The obtained nanosphere pellet was redispersed using sonication, washed and further characterized for particle size, polydispersity index, zeta potential, %entrapment efficiency, %drug loading and scanning electron microscopy. The redispersed suspension of nanospheres were then freeze dried using (10% w/v) trehalose and stored at 4ºC until further use.

Fabrication of artemether loaded polymeric nanorods

The film stretching technique demonstrated by Champion et. al. was used for the preparation of artemether loaded nanorods. Film forming solution was prepared using 5% (w/v) PVA and 2.5% (w/v) glycerol in Milli-Q water. The redispersed nanospheres equivalent to 10mg of ART were added and mixed with 10mL of the film forming solution. The solution mixture was poured in a 6 x 6 (cm) glass mould and dried at room temperature for 24h to get a thin film. The film was then attached in the *in-house* prepared film stretching apparatus and stretched in one dimension. The film stretching was performed by two methods, i.e., the solvent treatment method and the heat treatment method. In case of solvent treatment method, the film was incubated in acetone for 15min in order to liquify the nanospheres. It was followed by stretching of the film. Whereas, in case of heat treatment method, the film was dipped in preheated silicon oil (65ºC) for a period of 15min. Post 15min of incubation, the film was stretched while still being in the preheated silicon oil. In both the cases the stretching rate was kept constant which was 10mm/min. Various parameters such as extent of stretching, incubation period, film thickness were optimized to observe their effects on the shape of nanoparticles. Post stretching, the film was dissolved in Milli-Q water. The solution mixture was centrifuged to yield the nanorods, which were washed and further freeze dried using 10% (w/v) trehalose. Figure 1 depicts the a) Schematic representation of the *in*-house prepared film stretching apparatus b) Image of film stretching assembly acquired by digital camera.

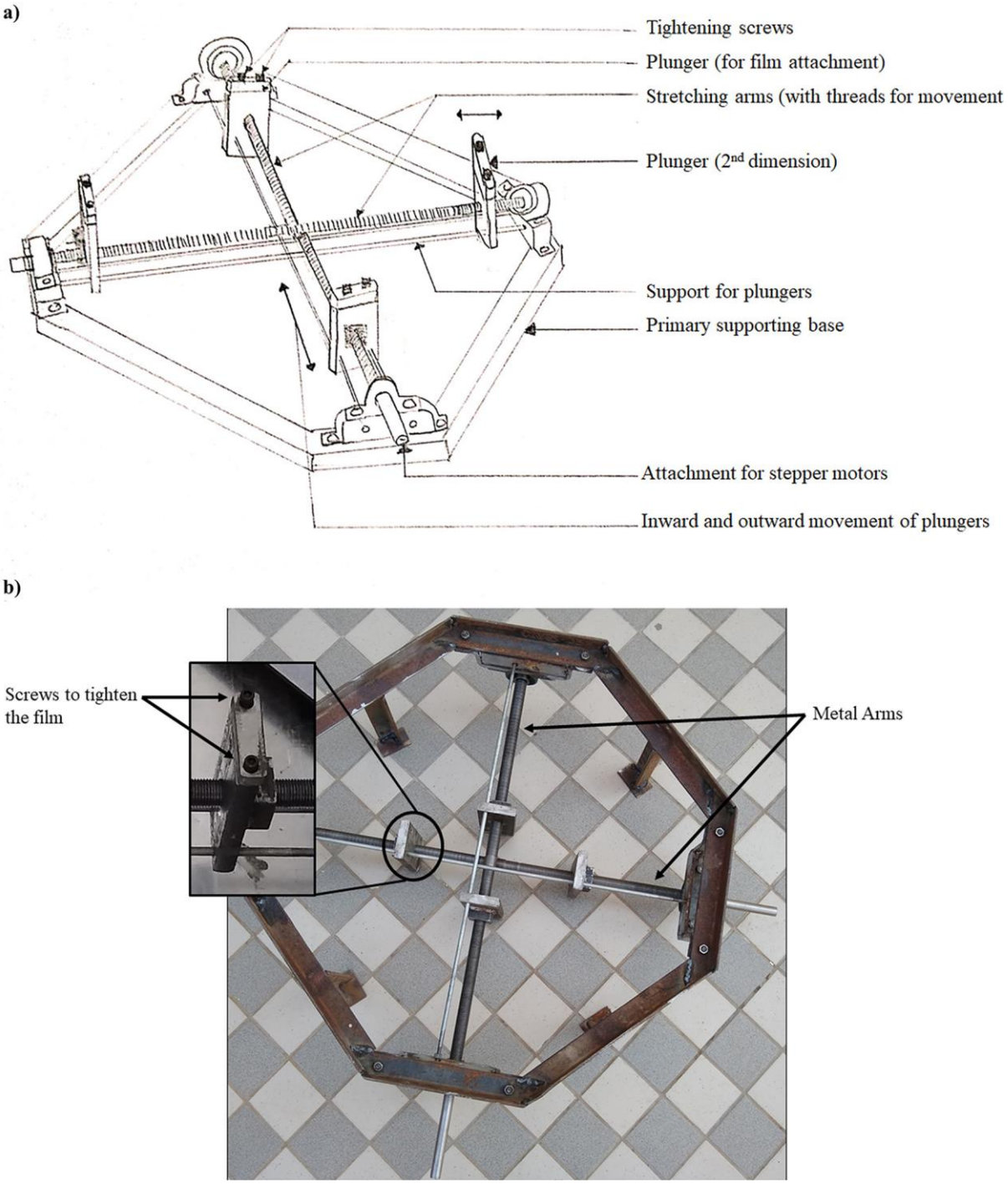

Figure 1. In house fabricated film stretching apparatus a) Schematic representation of the apparatus b) Image acquired by digital camera.

In vitro evaluation of artemether loaded polymeric nanorods

For characterization, nanospheres and nanorods were initially photographed by SEM by 45sec gold coating (Quorum Technologies Q150TES, East Sussex, England). The acquired images were analysed using ImageJ software to calculate the major axis, minor axis, aspect ratio, major Feret diameter and minor Feret diameter. Further, both the nanoformulations were characterised for the *in vitro* drug release by the dialysis bag method using 10mM phosphate buffer pH 7.4 with 1% (w/v) sodium lauryl sulphate. It was followed by cytotoxicity study using THP-1 monocyte cells with the MTT solution. Furthermore, the safety of the

nanoformulations was assessed by haemolysis study using fresh rat erythrocytes. It was followed by, the nanoparticle-erythrocyte interaction study using scanning electron microscopy and confocal microscopy by incubating the nanoformulations and erythrocytes together to understand the interaction of nanoparticles with the erythrocytes. Finally, the *in vitro* schizont maturation inhibition assay was conducted by treatment of short-term *in vitro* culture of *P. berghi* ANKA blood stages with different concentrations of ART and ART nanoformulations.

In vivo evaluation of artemether loaded polymeric nanorods

To understand the *in vivo* fate of the nanoformulations, pharmacokinetic study was performed on Sprague-Dawley rats (250-300g). Nanospheres and nanorods were administered intravenously in the rats and blood was collected from the retro orbital plexus at various time points till 24h followed by the analysis of ART content in the blood samples. The studies were carried out with four animals per group. Later, the biodistribution study was performed using the whole-body imaging of mice. DiR loaded nanospheres and nanorods were prepared as the same process mentioned above where ART was replaced by DiR in the organic phase. BALB/c mice were used for the study. The formulations were administered intravenously and the whole-body imaging was carried out at regular intervals till 24h. Finally, the antimalarial efficacy study was carried out in *P. berghi* infected BALB/c mice (6-8 weeks). The animals were induced with parasitaemia followed by treatment post 24h. On the basis of treatment, the animals were divided into different groups such as Group I (negative control), Group II (vehicle control; 0.9% normal saline), Group III (ART free drug), Group IV (blank nanospheres), Group V (ART loaded nanospheres), Group VI (Blank nanorods) and Group VII (ART loaded nanorods) which was continued till 4 days. Parasitaemia was analysed from blood withdrawn at predetermined time points from the animals.

Results

Fabrication of artemether loaded polymeric nanospheres

ART loaded polymeric nanospheres were prepared using the nanoprecipitation technique. Various optimization trials were performed which yielded particles of different size and drug content and are mentioned in table 1. The optimized nanosphere formulation yielded a particle size and polydispersity index of 129.3 ± 3.6 and 0.06 ± 0.01 respectively. The particles had a negatively charged surface with a value of -7.4 ± 0.69. And, the %EE and %DL were found to be 86.9 ± 0.2 and 10.2 ± 0.0 respectively.

Table 1. Particle size, PDI, %EE and zeta potential of the artemether loaded nanospheres

Composition					Particle size (nm)	PDI	Zeta potential (mV)	%EE	% DL
Artemether (mg)	PLGA (mg)	PVA (mg)	Acetone (mL)	Aqueous phase (mL)					
5	75	75	5	15	190.17 ± 18.01	0.06 ± 0.01	-7.98 ± 0.58	78.54 ± 1.76	4.91 ± 0.11
5	75	150	5	15	214.26 ± 6.23	0.238	-1.78 ± 0.22	79.98 ± 0.07	4.99 ± 0.00

10	75	300	10	30	196.8 ± 1.13	0.214	-2.16 ± 0.16	78.31 ± 0.02	9.21 ± 0.00
10	75	150	10	30	245.5 ± 44.54	0.183	-3.17 ± 0.24	80.58 ± 0.37	9.48 ± 0.04
10	75	150	15	30	129.33 ± 3.64	0.06 ± 0.01	-7.37 ± 0.69	86.87 ± 0.21	10.22 ± 0.02

Each value presented as mean ± SD, n=3

Fabrication of artemether loaded polymeric nanorods

The prepared nanospheres were embedded in the film to prepare nanorods. The characteristic parameters of nanorods prepared after different conditions are mentioned in table 2. Size-frequency distribution curve of major and minor axis of nanorods obtained from stretching of nanospheres after solvent treatment are presented in figure 2 (a-d) and figure 2 (e-h) respectively while the SEM images are presented in figure 2 (i-m). During the solvent treatment, the extent of stretching played a major role in the shape of the nanorods. When the film was stretched 2x of its initial length, the obtained nanorods had an aspect ratio of 2.1 ± 0.3. While, it was observed to be 3.8 ± 0.8 in case of the film stretched 4x of its initial length. The nanorods were observed to be uniformly elongated on the basis of its shape descriptor values ($D_{90\ major}$ = 170nm and $D_{90\ minor}$ = 75nm for 2x stretched film and $D_{90\ major}$ = 340 nm and $D_{90\ minor}$ = 75 nm for 4x stretched film). Film thickness also played a crucial role in presenting shape to the nanorods. The film of 150µm when stretched 4x of its initial length yielded nanorods of 5.1 ± 0.8. The increase in the aspect ratio was contributed by increase in the major axis and decrease in the minor axis. The particles were found to be elongated uniformly ($D_{90\ major}$ = 395 nm and $D_{90\ minor}$ = 80 nm for 150µm film). Finally, in case of PLGA 50:50, the nanorods were found to be uniformly elongated with an aspect ratio of 3.5 ± 0.7 ($D_{90\ major}$ = 300nm and $D_{90\ minor}$ = 80nm for PLGA 50:50). On the other hand, the nanospheres stretched after heat treatment had a greater aspect ratio as compared to the ones treated with solvent. The size-frequency distribution curve of major and minor axis of nanorods obtained from stretching of nanospheres after heat treatment are presented in figure 3 (a-c) and Fig. 3 (d-f) respectively while the SEM images are presented in figure 3 (g-j). An incubation time of 5min led to the formation of oval shaped nanorods with an aspect ratio of 1.72 ± 0.33 when the film was stretched 4x of its initial length. On the other hand, an incubation time of 15min led to the formation of elongated nanorods with an aspect ratio of 5.07 ± 0.92 ($D_{90\ major}$ = 355nm and $D_{90\ minor}$ = 195nm for film incubated for 5min and $D_{90\ major}$ = 700nm and $D_{90\ minor}$ = 130nm for film incubated for 15min). The film stretched 2x of its initial length led to the formation of nanorods with an aspect ratio of 3.60 ± 0.75 ($D_{90\ major}$ = 430nm and $D_{90\ minor}$ = 116nm for 2x stretched film). The %DL of the nanospheres and nanorods are mentioned in table 2. The %DL of nanorods was less as compared to nanospheres. It was presumed that the drug would have been lost during stretching and recovering of the nanorods.

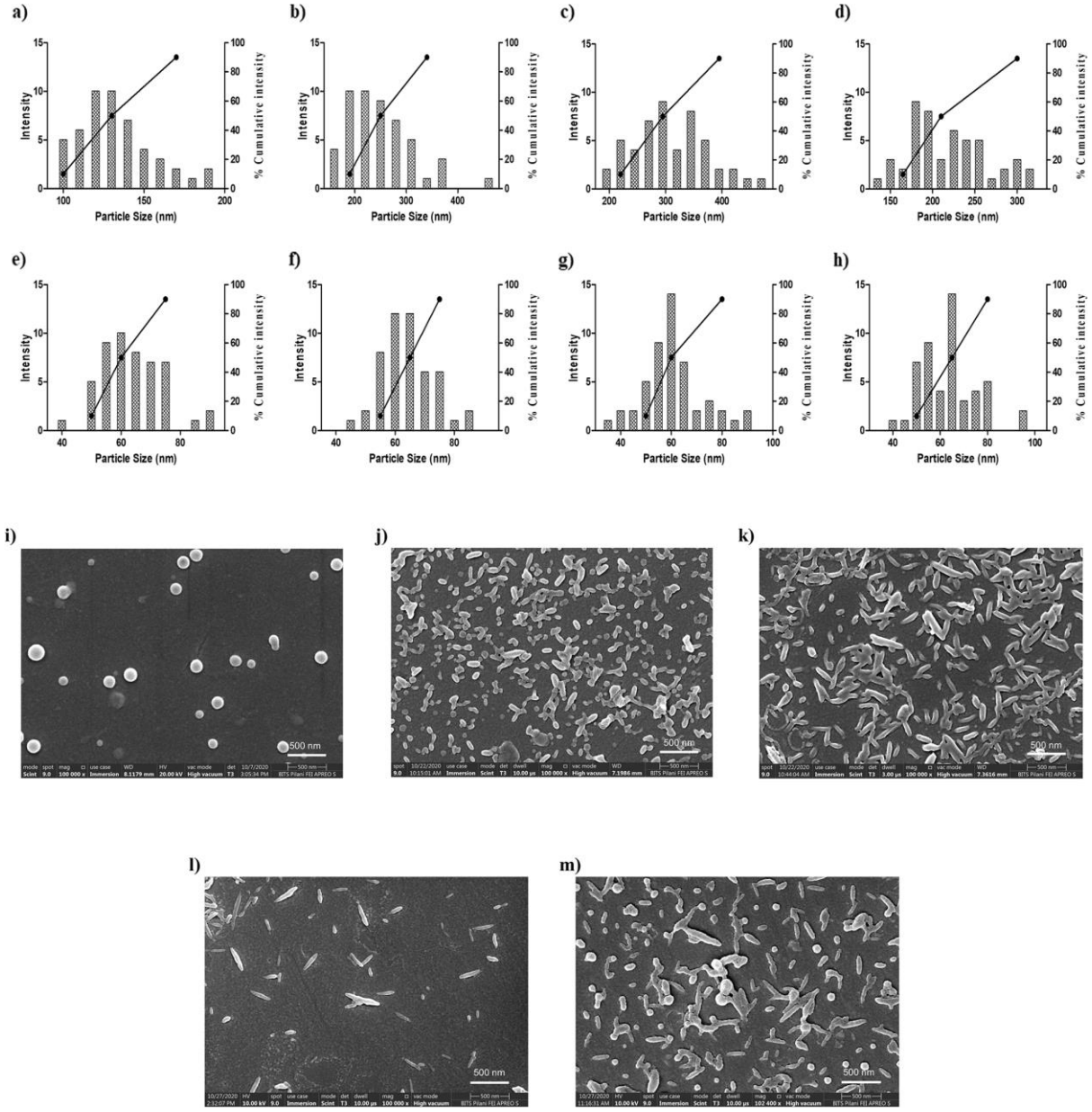

Figure 2. Characterisation of size and shape of the nanorods obtained from mechanical stretching of nanospheres after solvent treatment. Size-frequency distribution curves of major axis (a-d), minor axis (e-h) and SEM images (j-m) of nanorods, (i) of nanospheres; a) major axis, e) minor axis and j) SEM image of nanorods (film thickness = 100 µm, L/G ratio = 75: 25, stretching extent = 2x), b) major axis, f) minor axis and k) SEM image of nanorods (film thickness = 100 µm, L/G ratio = 75: 25, stretching extent = 4x), c) major axis, g) minor axis and l) SEM image of nanorods (film thickness = 150 µm, L/G ratio = 75: 25, stretching extent = 4x), d) major axis, h) minor axis and m) SEM image of nanorods (film thickness = 100 µm, L/G ratio = 50: 50, stretching extent = 4x).

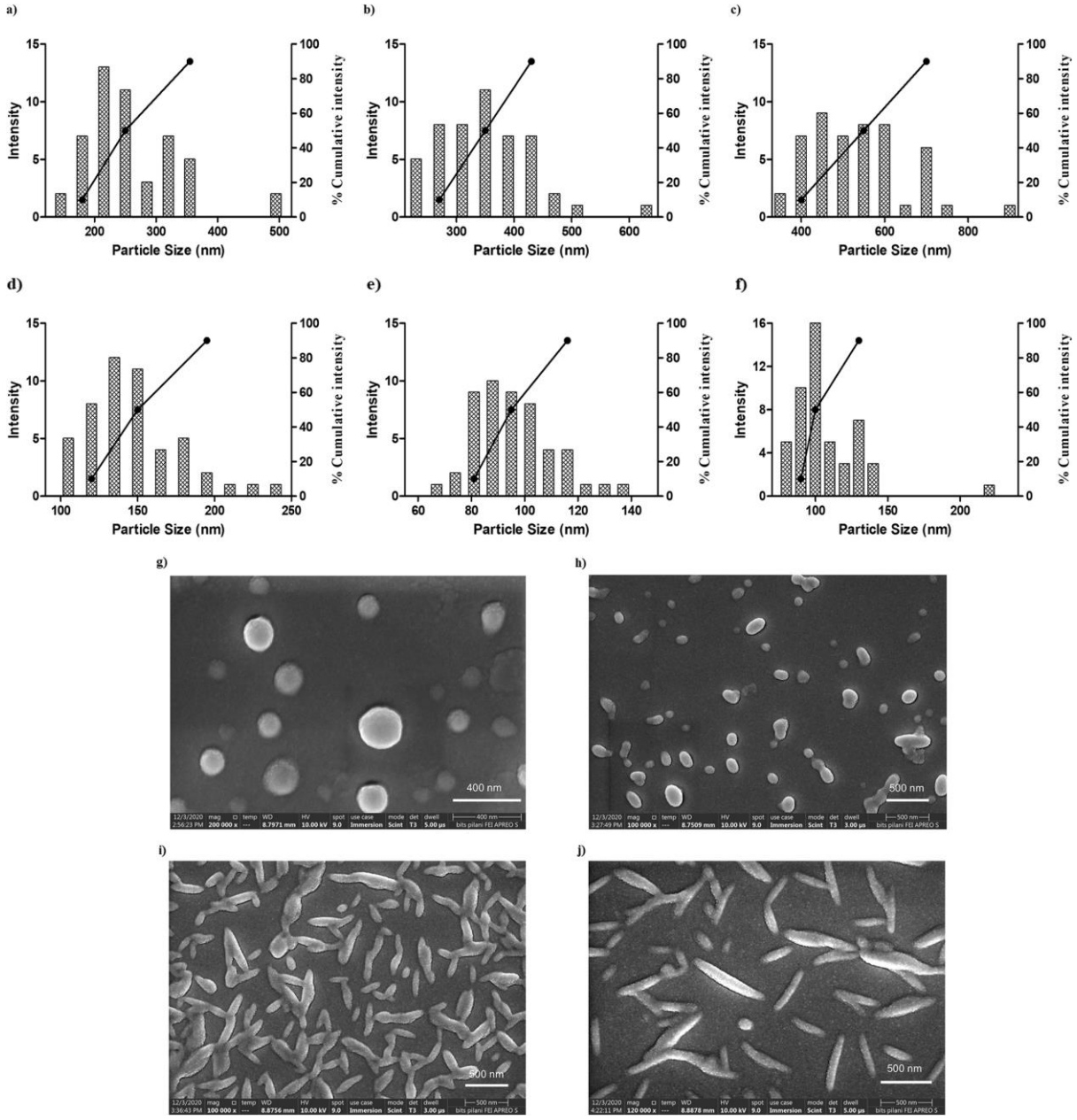

Figure 3. Characterisation of size and shape of the nanorods obtained from mechanical stretching of nanospheres after heat treatment. Size-frequency distribution curves of major axis (a-c), minor axis (d-f) and SEM images (h-j) of nanorods, (g) of nanospheres; a) major axis, d) minor axis and h) SEM image of nanorods (film thickness = 100 µm, L/G ratio = 75: 25, stretching extent = 4x, incubation time = 5 min), b) major axis, e) minor axis and i) SEM image of nanorods (film thickness = 100 µm, L/G ratio = 75: 25, stretching extent = 2x, incubation time = 15 min), c) major axis, f) minor axis and j) SEM image of nanorods (film thickness = 100 µm, L/G ratio = 75: 25, stretching extent = 4x, incubation time = 15 min).

In vitro evaluation of artemether loaded polymeric nanorods

The *in vitro* release study, it was observed that nanospheres and nanorods both present a sustained release of drug, however, nanorods result in a slower drug release as compared to nanospheres ($p < 0.05$). Although, at the end of 72h, both nanospheres and nanorods release around 85% of ART. The *in vitro* release profile is given in figure 4. While in the *in vitro* cytotoxicity study, ART free drug, ART loaded nanospheres and ART loaded nanorods were found to be non-toxic with a cell viability of more than 90% at ART content between 0.001 to

100µg/mL. While, at an ART equivalent concentration of 200µg/mL, all the three test samples were found to be toxic, although, ART loaded nanorods being the least toxic amongst them. The *in vitro* cytotoxicity profile is given in figure 4. In the *in vitro* haemolysis study, ART free drug, ART loaded nanospheres and ART loaded nanorods were found to be nonhemolytic at the concentrations between 0.001 to 200µg/mL. The *in vitro* haemolysis profile is given in figure 4. The erythrocyte-nanoparticle interaction study carried out using SEM and confocal microscope revealed that the nanospheres and nanorods both adhered to the erythrocytes however, the nanorods possessed greater surface area and higher contact angle which tends to require less bending energy thus interacting with the erythrocytes more as compared to the nanospheres. The *in vitro* erythrocyte nanoparticle interaction images using SEM and confocal microscopy is given in figure 5.

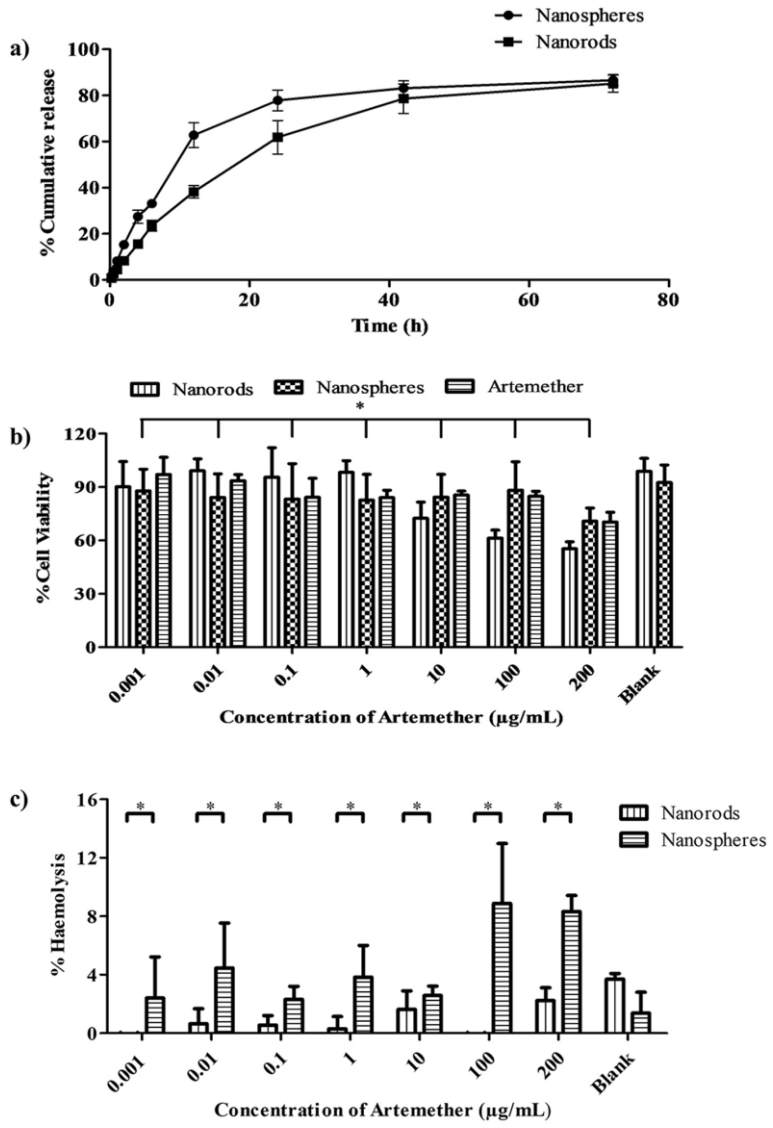

Figure 4. In vitro evaluation of nanospheres and nanorods a) In vitro release profile of nanosphere and nanorods in 50 ml of 10 mM phosphate buffer pH 7.4 with sodium lauryl sulphate (SLS) (1% w/v) for 72 h under stirring (100 rpm) at 37 C b) % cell viability of artemether loaded nanospheres, artemether loaded nanorods and artemether free drug at different artemether concentrations in THP-1 monocyte cell lines, c) % haemolysis of RBCs obtained from rat blood after treatment with artemether loaded nanospheres, artemether loaded nanorods at different artemether concentrations, Each data represents the mean ± SD; n = 3; * represents $p < 0.05$.

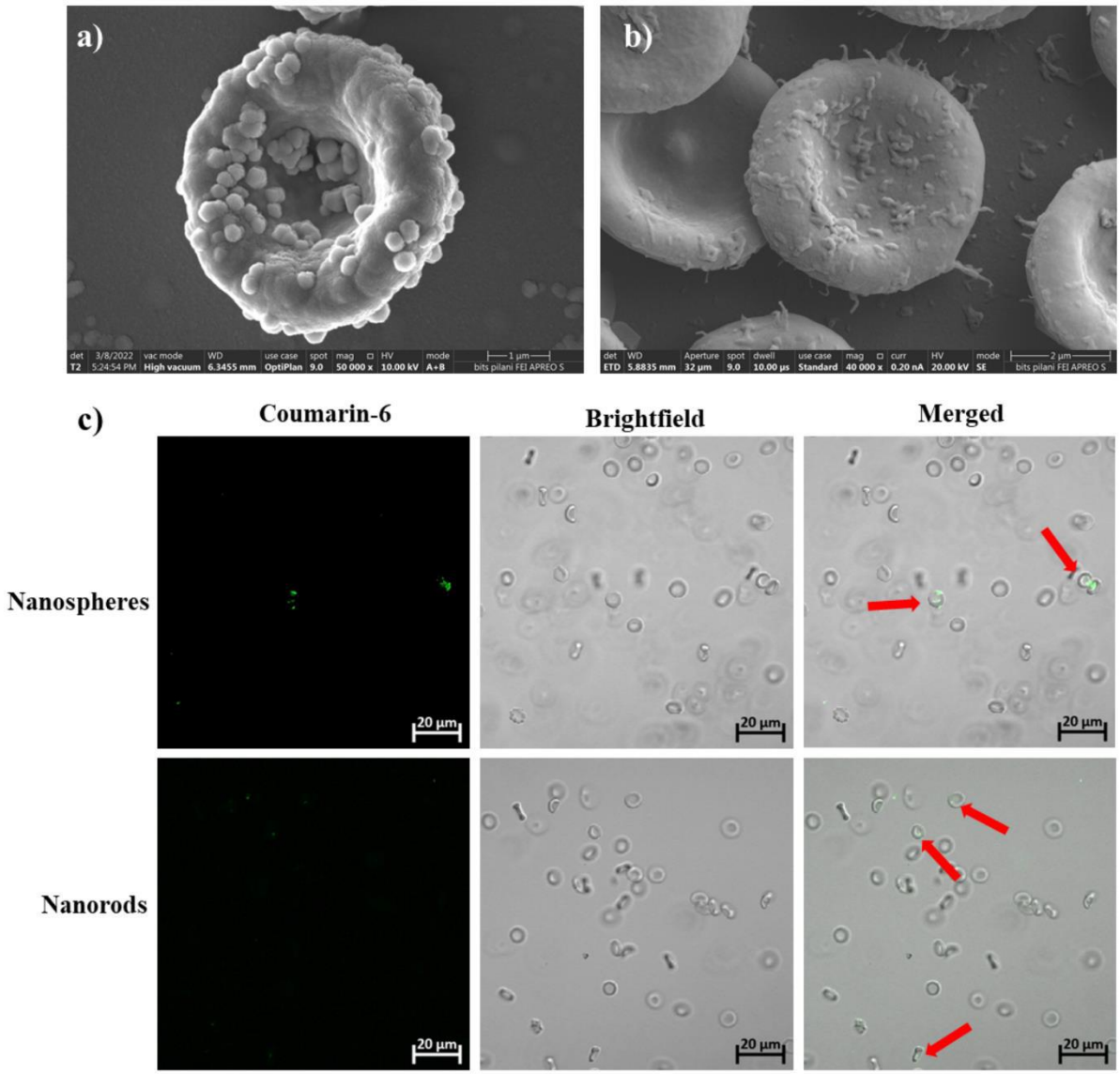

Figure 5. Erythrocyte nanoparticle interaction study. SEM image of a) nanospheres adsorbed on erythrocyte & b) nanorods adsorbed on erythrocytes; Confocal image of c) nanospheres and nanorods, adsorbed on erythrocyte

In the *in vitro* schizont maturation inhibition assay, ART loaded nanoformulations presented a concentration dependent inhibition of *P. berghei* schizont. ART free drug showed around 70% parasitic inhibition at all of the three treated concentrations (2, 4, 8µg/mL). At lower concentration (2µg/mL), ART loaded nanorods showed higher parasitic inhibition, on the other hand, at higher concentration (8µg/mL), ART loaded nanospheres presented a greater parasitic inhibition. The graphical representation of *in vitro* schizont maturation inhibition assay is presented in figure 6.

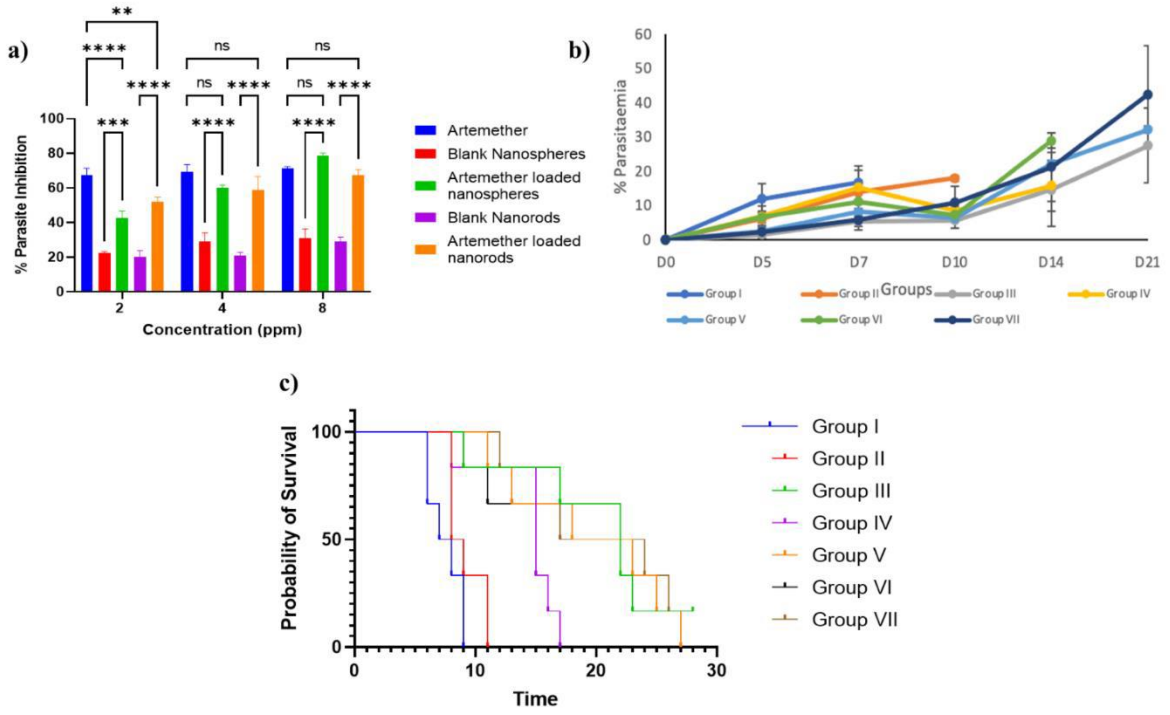

Figure 6. In vitro and in vivo antimalarial efficacy studies of artemether nanospheres and artemether nanorods a) In vitro schizont maturation inhibition by artemether, artemether nanospheres and artemether nanorods. Results are expressed as mean ± standard deviation (S.D.) and statistically checked by a two-way analysis of variance. The p-Value in comparison to artemether with other treatment groups, Blank nanospheres with artemether loaded nanospheres and Blank nanorods with artemether loaded rods are shown as ****p < 0.0001 to *p< 0.01 (significant), ns (non-significant). b) Percent parasitaemia observed in different treatment groups on different days (n=6). c) Kaplan-Meier analysis of mice in various experimental groups in suppressive test.

In vivo evaluation of artemether loaded polymeric nanorods

The *in vivo* pharmacokinetic studies, the C_{max} concentration of nanospheres was found to be 1.64-fold greater than nanorods. On the other hand, $t_{1/2}$ of nanorods was 3.09-fold higher than that of nanospheres. The AUC of nanorods was 1.8-folds greater than that of nanospheres which would result in greater exposure of the parasites towards the drug. While the clearance of nanorods was 2-fold lower than that of nanospheres. The parameters indicated that nanorods could maintain plasma drug concentrations for longer duration than the nanospheres. Pharmacokinetic profiles of artemether loaded nanospheres and artemether loaded nanorods are presented in figure 7. The *in vivo* biodistribution studies revealed that, at 30min, the concentrations of nanorods in the liver was significantly less than that of nanospheres probably due to the macrophage bypass. While after 24h, the intensity of nanorods in the abdominal region increased while that of the nanospheres decreased. This indicated that the nanorods eventually got deposited in the reticuloendothelial organs while in case of nanospheres, it was rapid. A comparative biodistribution profile of DIR loaded nanospheres and nanorods after intravenous administration is presented in figure 8.

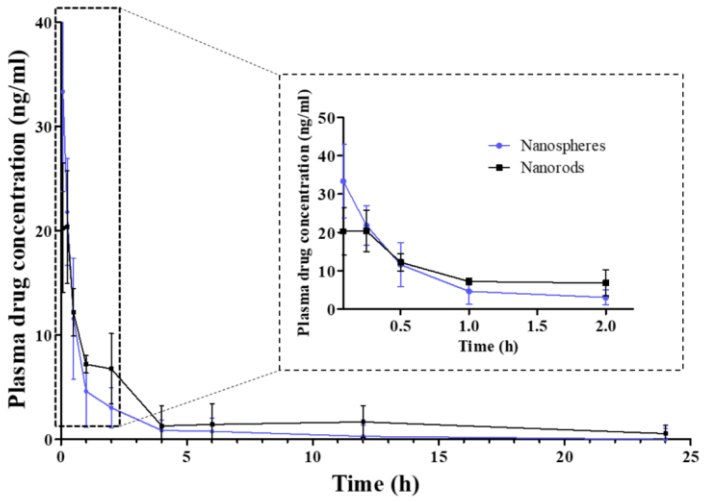

Figure 7. Pharmacokinetic profile of nanospheres (blue) and nanorods (black) after intravenous administration of artemether loaded nanospheres and artemether loaded nanorods

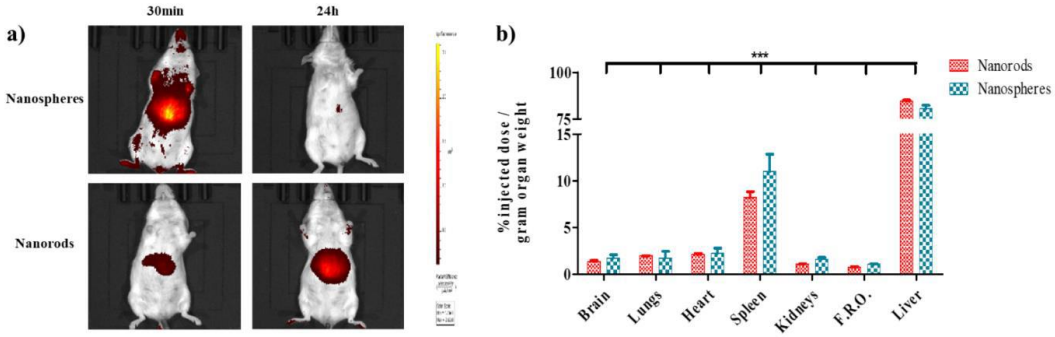

Figure 8. Biodistribution study of DiR loaded nanoformulations. a) Whole-body images of BALB/c mice after intravenous administration of nanospheres and nanorods; b) comparative biodistribution profile of nanospheres and nanorods.

The *in vivo* suppressive study, high parasitaemia was observed in the untreated group, the vehicle control group and the groups administered with blank nanospheres and blank nanorods. In case of ART loaded nanospheres, parasite suppression of around 78.46% on the 5th day while 51.40% on the 7th day was observed which indicated efficient chemo-suppression. While, in case of ART loaded nanorods, an increased chemo-suppression of 79.80% and 65.01% on day 5 and day 7 respectively was observed. The sustained drug release of ART would likely be responsible for its greater chemo-suppression. In case of free drug, 5.44 ± 1.46% parasitaemia was observed on 5th day which increased to 27.49±10.93% on 21st day causing animal death. The graphical representation of *in vivo* suppressive study on the basis of %parasitaemia is given in figure 6. The mice from the infected control group and vehicle control group died on 7th and 10th day respectively. The mice administered with blank nanoformulations also died within 21 days indicating no effect of the excipients. Only the animals treated with ART and ART loaded nanoformulations survived more than those of others with a significant difference. The survival graph of *in vivo* suppressive study is presented in figure 6.

Statistical Analysis

Data of all in vitro studies were represented as mean±SD with 3 biological replicates, while in vivo experiments were represented as mean±SEM with 4 biological replicates to obtain

statistically significant results. The results obtained were analyzed using Graphpad prism 6.01. Specific comparisons between two groups were performed using a student t-test with $p<0.05$ as a minimal level of significance. Mathematical fit functions were performed by ANOVA analysis.

Discussion

Malaria parasite resides in the erythrocytes of the host. Inside the erythrocytes, it proliferates, multiplies thus eventually destroying the cell which is followed by infection of another erythrocyte. Hence it is desirable for the drug delivery system to be present in the circulation maintaining plasma drug concentrations and be directly in contact with the erythrocytes. Nonspherical nanoparticles, when administered *in vivo* exhibit tumbling in the blood flow thus eventually causing movement towards the periphery of the blood vessel known as 'margination'. Margination of the nanoparticles may result in comparatively longer circulation time. The longer circulation time may also present greater chances of adhesion of the nonspherical nanoparticles to the endothelial cells of the vessels due to their higher contact angle.

In this study, we initially prepared nanospheres by nanoprecipitation method. It was observed that the size of the nanospheres increased as the ratio of organic phase to aqueous phase increased (1:2 to 1:3). This might be due to the less available organic solvent for the polymer during the formation of organic to aqueous solution mixture, thus resulting in precipitation of larger nanospheres with higher polydispersity. Further nanorods were prepared with the film stretching method. It was observed that parameters such as film thickness, extent of stretching, time of incubation of nanosphere liquification and polymer type played a major role in the fabrication of shape to the nanorods. The nanospheres would turn to nanorods when the polymeric cohesive forces would be superseded by the adhesive forces between the polymer of nanosphere and the film polymer. These forces would be the result of film stress applied on the film. The solvent treatment and the heat treatment would lead to the decrease in the cohesive forces thus promoting the elongation of nanospheres to nanorods. Increase in the film thickness resulted in increase in the major axis bud did not result in decrease in the minor axis which could be due to the higher stress caused by the film towards the nanorods in one dimension. While in case of PLGA 50:50 nanospheres, the nanorods formed had less aspect ratio than that formed by PLGA 75:25. As PLGA 50:50 has a greater viscosity it was thought that it might have contributed to greater resistance towards stretching thus causing nanorods of less AR. The incubation of 5min caused the formation of nanorods with less AR as compared to the ones incubated for 15min. It might be attributed to increased liquefication of nanospheres after 15min thus decreasing their viscosity, thus eventually presenting lesser strain while stretching.

Considering the drug release, the nanospheres present less surface area as compared to the nanorods. However, it was observed that the nanorods presented slower release than nanospheres. It might be due to the specific alignment of nanorods towards the periphery of the dialysis bag due to their greater surface area and contact angle. The specific alignment could lead to the formation of a stagnant layer around the nanorods causing a barrier towards the sink condition maintaining media thus leading to a lower release of the drug. Nanorods were found to be less cytotoxic and haemolytic. It might be due to the shape of the nanorods which, due to greater contact angle presents less membrane bending energy for interaction resulting in less cytotoxic and haemolytic. In the *in vitro* schizont maturation inhibition assay,

at higher concentration the nanospheres displayed greater parasitic inhibition. This might be attributed to the slower release of drug from the nanorods thus resulting in delayed attention of C_{max} in the culture media. In case of *in vivo* pharmacokinetic studies, the nanorods presented a more sustained release action thus maintain plasma drug concentration for a longer time. It might be attributed to the phagocyte uptake bypass and the margination of nanorods thus resenting this effect. The same observation was backed by the biodistribution studies where the nanorods deposition in the RES organs was slower than that of nanospheres. Nanorods displayed greater efficacy in treating the *P. berghei*-infected mice when compared to nanospheres. It can be attributed to the longer circulation of nanorods thus maintaining the plasma drug concentration for a longer time resulting in improved efficacy.

Impact of the research in the advancement of knowledge or benefit to mankind

Current strategy involves the delivery of artemether, an antimalarial drug with a short half-life with rod-shaped polymeric nanoparticles with intravenous rote. The drug is active against all erythrocytic stages of the parasite and is widely recommended as first line therapy in the malaria endemic countries. Current approved delivery strategy involves a tablet (Coartem®) with a combination of artemether and lumefantrine and an intravenous injection of artesunate. Coartem® suffers from an erratic absorption behaviour, high pill burden and complicated dosage regimen. While artesunate maintains the plasma drug concentration for a very short duration. Hence, artemether loaded nanorods which have demonstrated its capability of maintaining the plasma drug concentration for longer period of time and with an administration route which presents maximal bioavailability and is suitable for all categories of affected patients. Further, the nanoformulation can decrease the chances of disease recrudescence due to its property of maintaining the plasma drug concentrations for longer period of time. If implemented on a large scale, the delivery system might contribute in the reduction of the global malaria burden in patients of all age groups and complications.

Furthermore, the platform strategy of non-spherical drug delivery can prove to be suitable for other diseases and disorders and can be a suitable contestant in the upcoming novel drug delivery systems for long-acting drug delivery.

Literature references

(1) *Global Health Estimates 2019: Estimated deaths by age, sex, and cause*. https://www.who.int/data/gho/data/themes/mortality-and-global-health-estimates/ghe-leading-causes-of-death (Assessed on 01/08/2022).

(2) *Malaria*. https://www.who.int/news-room/fact-sheets/detail/malaria (Assessed on 22/08/2022).

(3) Richards, J. S.; Beeson, J. G. The Future for Blood-stage Vaccines against Malaria. *Immunol Cell Biol* **2009**, *87* (5), 377–390. https://doi.org/10.1038/icb.2009.27.

(4) *Global Malaria Programme*. https://www.who.int/teams/global-malaria-programme/guidelines-for-malaria (Assessed on 22/08/2022).

(5) Bhadra, D.; Bhadra, S.; Jain, N. K. Pegylated Lysine Based Copolymeric Dendritic Micelles for Solubilization and Delivery of Artemether. *Journal of Pharmacy and Pharmaceutical Sciences* **2005**.

(6) Ma, Y.; Lu, T.; Zhao, W.; Wang, Y.; Chen, T.; Mei, Q.; Chen, T. Enhanced Antimalarial Activity by a Novel Artemether-Lumefantrine Lipid Emulsion for Parenteral Administration. *Antimicrob Agents Chemother* **2014**. https://doi.org/10.1128/AAC.01428-13.

(7) Isacchi, B.; Arrigucci, S.; Marca, G. la; Bergonzi, M. C.; Vannucchi, M. G.; Novelli, A.; Bilia, A. R. Conventional and Long-Circulating Liposomes of Artemisinin: Preparation, Characterization, and Pharmacokinetic Profile in Mice. *J Liposome Res* **2011**. https://doi.org/10.3109/08982104.2010.539185.

(8) Pawar, S.; Shende, P. Dual Drug Delivery of Cyclodextrin Cross-Linked Artemether and Lumefantrine Nanosponges for Synergistic Action Using 23 Full Factorial Designs. *Colloids Surf A Physicochem Eng Asp* **2020**. https://doi.org/10.1016/j.colsurfa.2020.125049.

(9) Nnamani, P. O.; Hansen, S.; Windbergs, M.; Lehr, C. M. Development of Artemether-Loaded Nanostructured Lipid Carrier (NLC) Formulation for Topical Application. *Int J Pharm* **2014**. https://doi.org/10.1016/j.ijpharm.2014.10.004.

(10) Prabhu, P.; Suryavanshi, S.; Pathak, S.; Sharma, S.; Patravale, V. Artemether–Lumefantrine Nanostructured Lipid Carriers for Oral Malaria Therapy: Enhanced Efficacy at Reduced Dose and Dosing Frequency. *Int J Pharm* **2016**, *511* (1), 473–487. https://doi.org/10.1016/j.ijpharm.2016.07.021.

(11) Jain, K.; Sood, S.; Gowthamarajan, K. Optimization of Artemether-Loaded NLC for Intranasal Delivery Using Central Composite Design. *Drug Deliv* **2015**, *22* (7), 940–954. https://doi.org/10.3109/10717544.2014.885999.

(12) Parashar, D.; Aditya, N. P.; Murthy, R. S. R. Development of Artemether and Lumefantrine Co-Loaded Nanostructured Lipid Carriers: Physicochemical Characterization and in Vivo Antimalarial Activity. *Drug Deliv* **2016**, *23* (1), 123–129. https://doi.org/10.3109/10717544.2014.905883.

(13) Vanka, R.; Kuppusamy, G.; Praveen Kumar, S.; Baruah, U. K.; Karri, V. V. S. R.; Pandey, V.; Babu, P. P. Ameliorating the in Vivo Antimalarial Efficacy of Artemether Using Nanostructured Lipid Carriers. *J Microencapsul* **2018**, *35* (2), 121–136. https://doi.org/10.1080/02652048.2018.1441915.

(14) Patil, S.; Joshi, M.; Pathak, S.; Sharma, S.; Patravale, V. Intravenous β-Artemether Formulation (ARM NLC) as a Superior Alternative to Commercial Artesunate Formulation. *Journal of Antimicrobial Chemotherapy* **2012**. https://doi.org/10.1093/jac/dks293.

(15) Prabhu, P.; Suryavanshi, S.; Pathak, S.; Patra, A.; Sharma, S.; Patravale, V. Nanostructured Lipid Carriers of Artemether–Lumefantrine Combination for Intravenous Therapy of Cerebral Malaria. *Int J Pharm* **2016**. https://doi.org/10.1016/j.ijpharm.2016.09.008.

(16) Chadha, R.; Gupta, S.; Pathak, N. Artesunate-Loaded Chitosan/Lecithin Nanoparticles: Preparation, Characterization, and in Vivo Studies. *Drug Dev Ind Pharm* **2012**, *38* (12), 1538–1546. https://doi.org/10.3109/03639045.2012.658812.

(17) Gérard Yaméogo, J. B.; Mazet, R.; Wouessidjewe, D.; Choisnard, L.; Godin-Ribuot, D.; Putaux, J. L.; Semdé, R.; Gèze, A. Pharmacokinetic Study of Intravenously Administered Artemisinin-Loaded Surface-Decorated Amphiphilic γ-Cyclodextrin Nanoparticles. *Materials Science and Engineering C* **2020**, *106* (April 2019), 110281. https://doi.org/10.1016/j.msec.2019.110281.

(18) Mangrio, F. A.; Dwivedi, P.; Han, S.; Zhao, G.; Gao, D.; Si, T.; Xu, R. X. Characteristics of Artemether-Loaded Poly(Lactic-Co-Glycolic) Acid Microparticles Fabricated by Coaxial Electrospray: Validation of Enhanced Encapsulation Efficiency and Bioavailability. *Mol Pharm* **2017**. https://doi.org/10.1021/acs.molpharmaceut.7b00862.

(19) Aditi, S.; Kanchan, B.; Sneha, Za.; Munna, A.; Niroshini, N.; Kamalinder, S. Serum Albumin Nanoparticles for Effective Control of Malaria-Infected Erythrocytes. *Nanomedicine(Lond.)* **2016**, *11* (21), 2809–2828.

(20) Yaméogo, J. B. G.; Gze, A.; Choisnard, L.; Putaux, J. L.; Gansané, A.; Sirima, S. B.; Semdé, R.; Wouessidjewe, D. Self-Assembled Biotransesterified Cyclodextrins as Artemisinin Nanocarriers - I: Formulation, Lyoavailability and in Vitro Antimalarial Activity Assessment. *European Journal of Pharmaceutics and Biopharmaceutics* **2012**. https://doi.org/10.1016/j.ejpb.2011.12.007.

(21) Champion, J. A.; Mitragotri, S. Shape Induced Inhibition of Phagocytosis of Polymer Particles. *Pharm Res* **2009**. https://doi.org/10.1007/s11095-008-9626-z.

(22) Dasgupta, S.; Auth, T.; Gompper, G. Shape and Orientation Matter for the Cellular Uptake of Nonspherical Particles. *Nano Lett* **2014**. https://doi.org/10.1021/nl403949h.

(23) Jurney, P.; Agarwal, R.; Singh, V.; Choi, D.; Roy, K.; Sreenivasan, S. v.; Shi, L. Unique Size and Shape-Dependent Uptake Behaviors of Non-Spherical Nanoparticles by Endothelial Cells Due to a Shearing Flow. *Journal of Controlled Release* **2017**. https://doi.org/10.1016/j.jconrel.2016.11.033.

(24) Zhu, X.; Vo, C.; Taylor, M.; Smith, B. R. Non-Spherical Micro- and Nanoparticles in Nanomedicine. *Materials Horizons*. 2019. https://doi.org/10.1039/c8mh01527a.

(25) Yoo, J. W.; Doshi, N.; Mitragotri, S. Endocytosis and Intracellular Distribution of PLGA Particles in Endothelial Cells: Effect of Particle Geometry. *Macromol Rapid Commun* **2010**. https://doi.org/10.1002/marc.200900592.

Nominee

Atharva Rajendra Bhide
Ph.D. Research Scholar
Department of Pharmacy,